# Spin-Orbit Dimers and Noncollinear Phases in d1 Cubic Double Perovskites


doi: info:doi/10.1103/PhysRevLett.118.217202

# Spin-Orbit Dimers and Noncollinear Phases in $d^1$ Cubic Double Perovskites

Judit Romhányi,[1,2] Leon Balents,[3] and George Jackeli[1,4,*]
[1]Max Planck Institute for Solid State Research, Heisenbergstrasse 1, D-70569 Stuttgart, Germany
[2]Okinawa Institute of Science and Technology Graduate University, Onna-son, Okinawa 904-0395, Japan
[3]Kavli Institute for Theoretical Physics, University of California, Santa Barbara, California 93106, USA
[4]Institute for Functional Matter and Quantum Technologies, University of Stuttgart, Pfaffenwaldring 57, D-70569 Stuttgart, Germany
(Received 21 November 2016; published 26 May 2017)

We formulate and study a spin-orbital model for a family of cubic double perovskites with $d^1$ ions occupying a frustrated fcc sublattice. A variational approach and a complementary analytical analysis reveal a rich variety of phases emerging from the interplay of Hund's rule and spin-orbit coupling. The phase digram includes noncollinear ordered states, with or without a net moment, and, remarkably, a large window of a nonmagnetic disordered spin-orbit dimer phase. The present theory uncovers the physical origin of the unusual amorphous valence bond state experimentally suggested for $Ba_2BMoO_6$ ($B$ = Y, Lu) and predicts possible ordered patterns in $Ba_2BOsO_6$ ($B$ = Na, Li) compounds.

DOI: 10.1103/PhysRevLett.118.217202

Conventionally, frustration, low dimensionality, and low spin are the key attributes of emerging novel quantum ground states. In the quest to realize a quantum spin liquid, a state of spins possessing massive quantum entanglement and lacking magnetic order, researchers have extensively studied Mott insulators with antiferromagnetic (AFM) interactions on geometrically frustrated triangular, kagome, hyperkagome, and pyrochlore lattices [1,2]. Another route to frustration in Mott insulators with unquenched angular momentum is provided by orbital degrees of freedom. The directional character of degenerate $d$ orbitals may frustrate the magnetic interactions even on bipartite lattices and lead to a plethora of emergent phases with unusual spin patterns [3,4] or without long-range spin or orbital order [5–10].

In $4d$ and $5d$ transition metal compounds, the enhanced spin-orbit coupling (SOC), compared to $3d$ systems, fully or partly lifts the local degeneracy of a $d$ shell. When degeneracy is fully lifted, e.g., in the case of a single hole in a $t_{2g}$ shell, the anisotropic orbital interactions as well as related frustration are transferred to pseudospin one-half Kramers doublets of $d^5$ ions [4,11,12]. However, in the case of only partially lifting the degeneracy, the directional character of the electron density of the degenerate states is preserved, resulting in an effective reduction of magnetic sublattice dimensionality and strongly amplifying the effects of geometrical frustration. The Mott insulating $d^1$ double perovskites with undistorted cubic structure, such as spin-1/2 $Ba_2BMoO_6$ ($B$ = Y, Lu) and $Ba_2BOsO_6$ ($B$ = Na, Li), in which the only magnetically active ions, $Mo^{5+}$ or $Os^{7+}$, reside on a weakly frustrated fcc sublattice, well exemplify this physical scenario [13].

The osmium compounds $Ba_2NaOsO_6$ and $Ba_2LiOsO_6$ order magnetically [14–16]. Small effective local moments $\sim 0.7\ \mu_B$, compared to the spin-only value $1.7\ \mu_B$, have been extracted from high temperature susceptibilities in both materials [14]. The strong reduction of local moments is a direct manifestation of unquenched orbital momentum and strong SOC in the $5d$ shell of the $Os^{7+}$ ion [17–19]. In $Ba_2NaOsO_6$, an anomalously small net ordered moment $\sim 0.2\ \mu_B$ has additionally been detected [15,16]. Recent NMR measurements indicate a canted AFM order in the Na compound [20].

The reported experimental data on $Ba_2YMoO_6$ are even more puzzling: this compound does not show any structural or magnetic transition down to 50 mK [21–23]. The total high temperature entropy extracted from electronic heat capacity was reported to be close to $R \ln 4$ [22], indicating the presence of an extra twofold orbital degeneracy in addition to the spin, and allowing for the emergence of multiorbital physics. Based on magnetic susceptibility and muon spin rotation data, a valence bond glass state, an amorphous arrangement of spin singlets, has been proposed for $Ba_2YMoO_6$ [22], which remains quite stable against isovalent substitutions of $Ba^{2+}$ with $Sr^{2+}$ [24]. The magnetic susceptibility of a very similar compound, $Ba_2LuMoO_6$, also did not exhibit any magnetic transition down to 2 K [25]. Theoretically, various exotic phases, including multipolar order [13] and chiral spin-orbital liquid [26], have been put forward as possible candidates.

In this Letter, we introduce and study a spin-orbital model and show that a dimer-singlet phase, composed of random arrangement of spin-orbit dimers, without any type of long-range order is a natural ground state of the model. The physical properties of this disordered phase are consistent with all available experimental findings on molybdenum double perovskites. In addition, the minimal model supports complex noncollinear, coplanar, ordered patterns. We argue that such four-sublattice ordered states are realized in osmium compounds.

*Local electronic structure.*—The single $d$ electron of a $Mo^{5+}$ or $Os^{7+}$ ion in a cubic environment occupies the $t_{2g}$ manifold of degenerate $xy$, $xz$, $yz$ orbitals. It carries an effective angular momentum $l = 1$ with $|l^z = 0\rangle \equiv |xy\rangle$,

 

$|l^z = \pm 1\rangle \equiv (-1/\sqrt{2})(i|xz\rangle \pm |yz\rangle)$ [27]. The sixfold degeneracy of the local Hilbert space is lifted by the local SOC $H_{so} = -\lambda \vec{l} \cdot \vec{S}$, stabilizing the $j = l + S = \frac{3}{2}$ quartet and pushing the $j = \frac{1}{2}$ Kramers doublet to a higher energy. Here, $\vec{S}$ is an electron spin operator and $\lambda$ denotes the SOC. The states $j^z = \pm\frac{1}{2}$ of the $j = \frac{3}{2}$ manifold have predominantly $xy$ character, while $j^z = \pm\frac{3}{2}$ components are given by the superposition of $xz$ and $yz$ orbitals only [see Fig. 1(a)]. When SOC is much smaller (larger) than the exchange interactions between neighboring ions, it is more convenient to use the $t_{2g}$ ($j = \frac{3}{2}$) basis. The following analysis covers both limits.

*Spin-orbital Hamiltonian.*—In the double perovskite structure, each nearest-neighbor bond of the fcc sublattice of magnetic ions belongs to one of the crystallographic planes $xy$, $xz$, or $yz$, as shown in Fig. 1(b). We label these bonds as well as the $t_{2g}$ orbitals with a cubic axis $\gamma(=a, b, c)$ normal to their planes; e.g., $xy$ becomes $c$. The hopping between neighboring $t_{2g}$ orbitals takes place through the intermediate oxygens' $p$ orbitals, or direct hybridization. Along a $\gamma$-type bond the dominant overlap, with amplitude $t$, is between $\gamma$ orbitals [13,28]. The low-energy spin-orbital model is obtained via standard second order perturbation theory in $t/U$ ($U$ being the local Coulomb repulsion) [29], and reads as follows:

$$\mathcal{H} = \sum_{\langle ij\rangle_\gamma} \left[ -J_1 \left( \vec{S}_i \cdot \vec{S}_j + \frac{3}{4} \right) + J_2 \left( \vec{S}_i \cdot \vec{S}_j - \frac{1}{4} \right) \right] P_{ij}^{(\gamma)} + J_3 \sum_{\langle ij\rangle_\gamma} \left( \vec{S}_i \cdot \vec{S}_j - \frac{1}{4} \right) \bar{P}_{ij}^{(\gamma)} - \lambda \sum_i \vec{l} \cdot \vec{S}. \quad (1)$$

$\langle ij\rangle_\gamma$ denotes a $\gamma$-type bond, $J_{1(2)} = \frac{1}{4} J r_{1(2)}$, $J_3 = \frac{1}{3} J (2r_2 + r_3)$, $J = 4t^2/U$, the set of $r_n$ describing the multiplet structure of excited states are functions of $\eta = J_H/U \ll 1$ [31], and $J_H$ is Hund's coupling.

The isotropic spin exchange couplings depend on the orbital occupancy of the corresponding bonds [3,32], and are described by the first three terms of Eq. (1), with the orbital projectors $P_{ij}^{(\gamma)} = n_i^{(\gamma)}(1 - n_j^{(\gamma)}) + (1 - n_i^{(\gamma)}) n_j^{(\gamma)}$ and $\bar{P}_{ij}^{(\gamma)} = n_i^{(\gamma)} n_j^{(\gamma)}$, where $n_i^{(\gamma)}$ is the occupation number of a $\gamma$ orbital. The spin isotropy is broken by the SOC in Eq. (1), allowing symmetric anisotropic exchange between $j = \frac{3}{2}$ quartets. In cubic double perovskites, the antisymmetric Dzyaloshinsky-Moriya exchange is forbidden by the bond inversion symmetry.

*Dimer-singlet phase.*—We start our analysis by setting the small parameter $\eta = 0$, and we discuss later the model Eq. (1) in its full parameter space. We consider two limiting cases when $\lambda \ll J$ or $\lambda \gg J$, and identify the ground state phases of the model Eq. (1) through analytical considerations. At $\eta = 0$, the first three terms of the model Eq. (1)

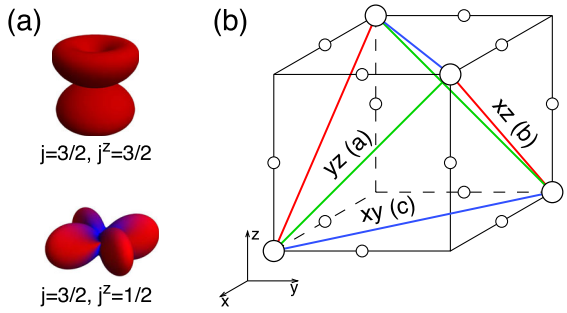


FIG. 1. (a) Density profile of $j = 3/2$ quartet. The states $j^z = \pm\frac{1}{2}$ (bottom) have dominant $xy$-orbital character, while $j^z = \pm\frac{3}{2}$ components (top) are composed of $xz$ and $yz$ orbitals. Red and blue coloring denotes the up and down spin distribution, respectively. (b) Crystallographic unit cell containing four molybdenum ions (large circles). Oxygen positions are indicated by small circles. The nearest-neighbor bonds belonging to different cubic planes are distinguished by different colors. The $t_{2g}$ orbitals active along the corresponding bonds are also indicated.

can be grouped, up to a constant term, into one [32], and the model simplifies to

$$\mathcal{H} = J \sum_{\langle ij\rangle_\gamma} \left( \vec{S}_i \cdot \vec{S}_j + \frac{1}{4} \right) \bar{P}_{ij}^{(\gamma)} - \lambda \sum_i \vec{l} \cdot \vec{S}. \quad (2)$$

The expectation value of the first term in Eq. (2) in any classical, i.e., site-factorized, state is non-negative. At $\lambda = 0$, the zero minimum classical energy is achieved by forming decoupled layers of AFM square lattices with uniform planar orbital order. In this state, the orbital projectors $\bar{P}_{ij}^{(\gamma)} = 1$ (0) on intralayer (interlayer) bonds and $\langle \vec{S}_i \cdot \vec{S}_j \rangle = -\frac{1}{4}$ on intralayer bonds. Hence, orbital "flavors" are decoupled, and flipping locally an orbital flavor does not cost energy, resulting in a massive ground state degeneracy [32]. A product state constructed from entangled quantum spin-orbit states on decoupled dimer bonds has, however, lower negative energy, $\mathsf{E}_{\mathrm{DS}} = -\frac{1}{4} J$. This phase, termed here as the dimer-singlet phase, corresponds to a hard-core dimer covering of the fcc lattice, with $\bar{P}_{ij}^{(\gamma)} = 1$ (0) on (inter)dimer bonds. On a dimer bond, spins form a singlet and occupied orbitals have lobes directed along the bond. Covering the lattice with such dimers is in fact an exact eigenstate of the Hamiltonian Eq. (2). When neighboring dimers are in the same plane, an energetically unfavorable larger cluster of AFM coupled spins are formed [33], and such configurations are banned from the ground state manifold. Although this seems to be a rather strong constraint, the orientational degeneracy of dimer covering remains extensive [32].

For $\lambda \gg J$, the $t_{2g}$ levels are split and the components of the lower $j = 3/2$ quartet form the relevant basis, which we label by pseudospin $\vec{s}$ and pseudo-orbital $\vec{\tau}$ states: $|\tau^z = \frac{1}{2}, s^z = \pm\frac{1}{2}\rangle \equiv |j = \frac{3}{2}, j^z = \pm\frac{1}{2}\rangle$ and $|\tau^z = -\frac{1}{2}, s^z = \pm\frac{1}{2}\rangle \equiv |j = \frac{3}{2}, j^z = \pm\frac{3}{2}\rangle$ [34]. Projecting Eq. (2) onto this new basis, we find

$$\mathcal{H} = \tilde{J} \sum_{\langle ij \rangle_\gamma} \left( \vec{s}_i \cdot \vec{s}_j + \frac{1}{4} \right) \tilde{P}_{ij}^{(\gamma)}, \tag{3}$$

where $\tilde{P}_{ij}^{(\gamma)} = (\frac{1}{2} + \tau_i^{(\gamma)})(\frac{1}{2} + \tau_j^{(\gamma)})$, $\tilde{J} = \frac{4}{9} J$, $\tau^{(a)} = -\frac{1}{2}\tau^z - (\sqrt{3}/2)\tau^x$, $\tau^{(b)} = -\frac{1}{2}\tau^z + (\sqrt{3}/2)\tau^x$, and $\tau^{(c)} = \tau^z$. Hamiltonian Eq. (3) has the same form as the Kugel-Khomskii model of $e_g$ orbitals on a cubic lattice [3] and explicitly reveals the emergent, at large $\lambda$, hidden SU(2) symmetry pointed out in Ref. [13]. Similarly to $\lambda = 0$, the ground state manifold of Eq. (3) is spanned by dimer singlets, but now these are composed of pseudospins instead of real spins.

Insight for intermediate $\lambda$ can be gained by exactly solving the model Eq. (1) on an isolated bond, since the interdimer couplings appear to be much smaller than intradimer ones (see below). For each value of $\lambda$, we find the singlet ground state

$$|\bigcirc\!\!-\!\!\bigcirc\rangle = \left( |\Uparrow\Downarrow\rangle - |\Downarrow\Uparrow\rangle \right)/\sqrt{2}\,, \tag{4}$$

where the wave functions of pseudospins $\Uparrow(\Downarrow)$ depend on the strength of $\lambda$ [32]; e.g., in the $xy$ plane, we have

$$|\Uparrow(\Downarrow)\rangle = \cos\vartheta |0, \uparrow(\downarrow)\rangle + \sin\vartheta |(-)1, \downarrow(\uparrow)\rangle. \tag{5}$$

In the two limiting cases, $\lambda = 0$ and $\lambda \gg 1$, the variational parameter $\theta$ becomes 0 and $\arccos\sqrt{2/3}$, respectively. The SOC inflates the planar orbital, so that at large $\lambda$ it becomes $|j = \frac{3}{2}, j_z = \pm\frac{1}{2}\rangle$. The latter has small out-of-plane component, see Fig. 1(a), generating finite but small interactions between, otherwise decoupled, dimers. However, as it follows, interdimer couplings do not select any particular superstructure of dimers.

Figure 2 shows all possible interdimer bonds allowed in the ground state manifold. Such a bond may connect two dimers both perpendicular to the connecting bond itself; then, either the connected dimers belong to different planes ($\mathsf{b}_1$) or to the same plane ($\mathsf{b}_2$). The third possibility $\mathsf{b}_3$ is that one of the dimers is in the same plane as the interdimer bond, and the other is perpendicular to them [see Fig. 2]. Consequently, regardless of the dimer arrangements, each dimer has exactly six neighboring $\mathsf{b}_3$ bonds. Out of $6\mathcal{N}$ bonds of the fcc lattice with $\mathcal{N}$ sites, there are in total $\frac{1}{2}\mathcal{N}$ dimer bonds, $3\mathcal{N}$ $\mathsf{b}_3$-type, and remaining $\frac{5}{2}\mathcal{N}$ $\mathsf{b}_1$- or $\mathsf{b}_2$-type of bonds. Each dimer ($\mathsf{b}_n$-type) bond hosts a finite energy $\mathcal{E}_\mathsf{d}$ ($\mathcal{E}_{\mathsf{b}_n}$). As both $\mathsf{b}_1$ and $\mathsf{b}_2$ bonds connect dimers out of their plane, $\mathcal{E}_{\mathsf{b}_1} = \mathcal{E}_{\mathsf{b}_2}$ and the energy of a product dimer state,

$$\mathsf{E}_{\mathrm{DS}} = (\mathcal{E}_\mathsf{d} + 5\mathcal{E}_{\mathsf{b}_1} + 6\mathcal{E}_{\mathsf{b}_3})\mathcal{N}/2, \tag{6}$$

is independent of the dimer covering. Hence, the interdimer couplings do not order dimers and the massive orientational degeneracy persists. In real materials, however, a mis-site disorder and/or uncorrelated local distortions most likely select a random dimer covering, rendering the system to freeze in a glassy manner.

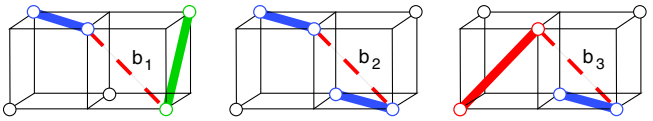


FIG. 2. Types of different interdimer bonds depicted as dashed lines. Dimers are represented with ○—○ and are colored according to three cubic planes they belong to. Bonds $\mathsf{b}_1$ and $\mathsf{b}_2$ couple dimers perpendicular to these bonds. Bond $\mathsf{b}_3$ connects a dimer from an orthogonal plane with another one that is in the same plane as $\mathsf{b}_3$ itself.

In an amorphous dimer-singlet phase, momenta of the excitations are not well defined, but their energies are. Moreover, the interdimer couplings are much smaller than the intradimer exchange, allowing an isolated dimer description of the bulk magnetic spectra. At $\eta$, $\lambda = 0$, as product dimer states are exact eigenstates, spins of different dimers are completely decoupled. In the large $\lambda$ limit, the interdimer pseudospin exchange $J' \simeq \frac{1}{16}\tilde{J} \ll \tilde{J}$. This estimate follows from Eq. (3) by noting that $\langle \tilde{P}_{ij}^{(\gamma)} \rangle = \frac{1}{16}$ on the interdimer bonds. Two types of local excitations allowed by magnetic dipole transitions are illustrated in Fig. 3. The upper one corresponds to flipping locally a (pseudo)spin at the energy cost $\Delta_S = J(\tilde{J})$ in small (large) $\lambda$ limit. The lower is a (pseudo-)orbital excitation that costs half the energy, $\Delta_O = \frac{1}{2}J(\frac{1}{2}\tilde{J})$, of a spinlike excitation. These estimates follow from the expectation values of the limiting Hamiltonians, Eqs. (2) and (3), in the ground state of an isolated bond, Fig. 3 (left), and its excited states, Fig. 3 (right). Using reported parameters for $Ba_2YMoO_6$ [29], we estimate the energy of spinlike (orbital-like) excitations $\Delta_{S(O)} \simeq 20$–$45\,(10$–$23)$ meV, for large-small SOC, and their bandwidth ($\sim J'$) of about few meV. In the magnetic dipolar channel, spinlike excitations carry stronger intensity than orbital-like ones. These findings agree well with neutron scattering data on powder samples, discussed below.

There are additional thermally accessible nonlocal excitations at lower energies. For example, AFM coupled spin clusters, or orphan spins, may emerge as a result of thermally induced orbital reorientation. An important

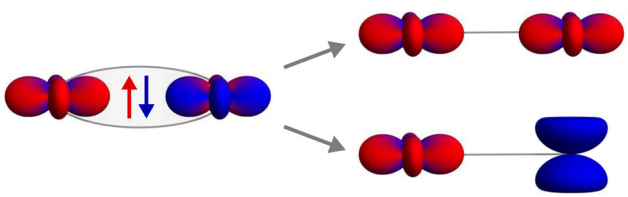

FIG. 3. Excitations of a spin-orbit dimer in the large $\lambda$ limit. Flipping locally, for example, the $j^z = -1/2$ component to $j^z = 1/2$ or to $j^z = -3/2$ corresponds to flipping the pseudospin (top) or pseudo-orbital (bottom), respectively. Local excitations for small SOC correspond to changing the real spins or orbitals.

difference between the well-studied spin-only dimer systems and our model is the lack of a hard gap. Here, on account of orbital degrees of freedom, the spectrum cannot be characterized by a single energy scale.

*Phase diagram.*—To explore the entire phase diagram of the full Hamiltonian Eq. (1), we used a site-factorized variational approach and compared the energies of ordered and dimer-singlet phases. The latter is numerically obtained from Eq. (6) using a product state of the exact wave functions of isolated dimers. Within our variational approach, the magnetic and crystallographic unit cells coincide; however, we still need 40 variational parameters to construct a trial wave function [32]. When $\eta = 0$, the ground state is a random arrangement of spin-orbit dimers (see inset in Fig. 4) for any value of $\lambda$. Only the nature of the pseudospins forming the singlet dimers is affected by $\lambda$, in accordance with the above analytical considerations. For large enough Hund's coupling, we find two noncollinear but coplanar phases of ordered total angular momenta $\vec{j}$ (see Fig. 4). One, termed here as coplanar FM, has a finite net moment along the [110] (or equivalent) direction, i.e., along one of the bonds, as experimentally observed [14]. The other, coplanar AFM, has no net moment. In the dimer-singlet phase, on a dimer bond in the $\gamma$ plane, a corresponding $\gamma$ orbital is predominately occupied, with occupancy decreasing from $n^{(\gamma)} = 1$ to $\frac{2}{3}$ with increasing $\lambda$. Hund's coupling induced transitions to ordered states are accompanied by complex rearrangements of an electron density within the SOC split $t_{2g}$ multiplet, with orbital occupancies dictated by the actual values of the parameters; e.g., in coplanar-AFM order in a cubic $\gamma$ plane the $\alpha$ and $\beta$ orbitals are predominantly occupied compared to the in-plane $\gamma$ orbital. All phase boundaries appear to be first order within our approach: the net moment and the order parameters drop to zero across the transitions from the coplanar-FM to the coplanar-AFM state and from the ordered to disordered dimer-singlet phase, respectively. However, one cannot rule out a second order symmetry allowed transition between ordered states, or an exotic continuous transition from a spontaneously dimerized phase to ordered states [35].

*Experimental implications.*—The dimer-singlet phase captures experimental observations on the molybdenum compounds. In agreement with experiments, it does not exhibit any long-range ordering nor break any global symmetry. Its extensive degeneracy explains the observed glassy behavior and suggests the presence of a residual entropy, that cannot be excluded based on heat capacity data [22]. Magnetic susceptibility and electronic heat capacity [22,23] suggest the presence of pseudogapped, rather than hard-gapped, low-energy excitations, consistent with the dimer-singlet phase. Neutron scattering experiments on powder samples [36] revealed excitations that are in line with the spectrum of weakly coupled spin-orbit dimers. An intense "mode" observed at $\Delta_S \simeq 28$ meV with

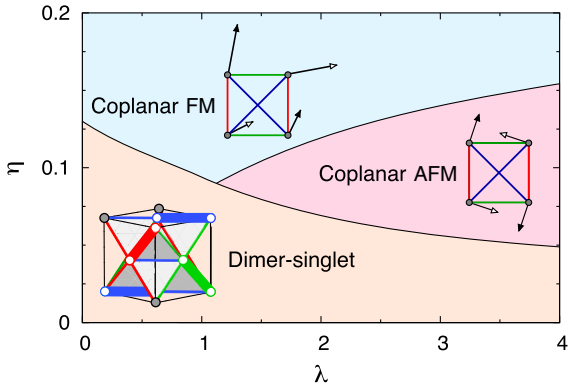


FIG. 4. Phase diagram of the model Eq. (1) as the function of Hund's coupling $\eta$ and the SOC $\lambda$ (in units of $J$). For small values of $\eta$ the dimer-singlet phase (see inset) is stable over the entire range of $\lambda$. With increasing Hund's coupling, noncollinear coplanar phases with ordered moments in one of the cubic planes are stabilized. The ferro-type coplanar state, coplanar FM, has a finite net moment pointing along the [110] (or equivalent) direction. The illustrations show a tetrahedron of four molybdenum sites projected onto the plane of ordered $\vec{j}$ moments, depicted as arrows.

bandwidth of about 4 meV is interpreted here as a (pseudo) spin singlet-to-triplet excitation. A less intense, lower-energy ($\Delta_O \simeq 9$–$17$ meV) response centered around half the energy of $\Delta_S$ is naturally attributed to (pseudo-)orbital excitation. These lower-lying excitations have also been observed in NMR response [21]. The energetics of the observed excitations agrees well with the above estimates, $\Delta_{S(O)} \simeq 20$–$45(10$–$23)$ meV. In addition, the infrared transmission spectra indicate the emergence of uncorrelated local distortions of $MoO_6$ octahedra below 130 K [37], at around the same temperature the magnetic susceptibility starts to decrease, most likely due to formation of spin-orbit dimers. In the dimer-singlet phase, such uncorrelated distortions emerge due to the directional character of the occupied orbitals.

The four-sublattice ordered states in the phase diagram (Fig. 4) may provide a description for the isostructural osmium compounds $Ba_2LiOsO_6$ and $Ba_2NaOsO_6$. The latter is characterized by very small net magnetic moment $\sim 0.2\ \mu_B$ along the [110] easy axis [14]. We find the net moment $\vec{M} = 2\vec{S} - \vec{l}$ along the same [110] (or equivalent) direction, being $\sim 1\ \mu_B$ for small and $\sim 0.1\ \mu_B$ for large $\lambda$.

To summarize, within a minimal microscopic model, we have proposed a unified theoretical description of possible ground states in $d^1$ cubic double perovskites. The obtained spin-orbital model shows a rich phase behavior including a massively degenerate dimer-singlet manifold, without any long-range order, and unusual noncollinear ordered patterns. Our theoretical study elucidates physics behind and provides explanations of experimental data on molybdenum- and osmium-based compounds. The physics discussed here may also be relevant to other heavy transition

metal compounds, such as molybdenum pyrochlores, in which a random distribution of "dimerized" bonds, induced by orbital degrees, have been recently revealed by pair-distribution function measurements [38].

We thank G. Chen, M. Haverkort, G. Khaliullin, F. Mila, W. Natori, J. A. M. Paddison, S. Streltsov, and H. Takagi for discussions. J. R. acknowledges funding from the Hungarian OTKA Grant No. K106047. Work by L. B. was supported by the DOE, Office of Science, Basic Energy Sciences under Award No. DE-FG02-08ER 46524. G. J. benefited from the facilities of the KITP, and was supported in part by the NSF under Grant No. NSF PHY11-25915.

*Also at: Andronikashvili Institute of Physics, 0177 Tbilisi, Georgia.

[1] L. Balents, Nature (London) **464**, 199 (2010).
[2] L. Savary and L. Balents, Rep. Prog. Phys. **80**, 016502 (2017).
[3] K. Kugel and D. Khomskii, Sov. Phys. Usp. **25**, 231 (1982).
[4] G. Khaliullin, Prog. Theor. Phys. Suppl. **160**, 155 (2005).
[5] H. F. Pen, J. van den Brink, D. I. Khomskii, and G. A. Sawatzky, Phys. Rev. Lett. **78**, 1323 (1997).
[6] G. Khaliullin and S. Maekawa, Phys. Rev. Lett. **85**, 3950 (2000).
[7] F. Vernay, K. Penc, P. Fazekas, and F. Mila, Phys. Rev. B **70**, 014428 (2004).
[8] S. Di Matteo, G. Jackeli, C. Lacroix, and N. B. Perkins, Phys. Rev. Lett. **93**, 077208 (2004).
[9] S. Di Matteo, G. Jackeli, and N. B. Perkins, Phys. Rev. B **72**, 024431 (2005).
[10] G. Jackeli and D. I. Khomskii, Phys. Rev. Lett. **100**, 147203 (2008).
[11] G. Chen and L. Balents, Phys. Rev. B **78**, 094403 (2008).
[12] G. Jackeli and G. Khaliullin, Phys. Rev. Lett. **102**, 017205 (2009).
[13] G. Chen, R. Pereira, and L. Balents, Phys. Rev. B **82**, 174440 (2010).
[14] K. Stitzer, M. Smith, and H.-C. zur Loye, Solid State Sci. **4**, 311 (2002).
[15] A. S. Erickson, S. Misra, G. J. Miller, R. R. Gupta, Z. Schlesinger, W. A. Harrison, J. M. Kim, and I. R. Fisher, Phys. Rev. Lett. **99**, 016404 (2007).
[16] A. J. Steele, P. J. Baker, T. Lancaster, F. L. Pratt, I. Franke, S. Ghannadzadeh, P. A. Goddard, W. Hayes, D. Prabhakaran, and S. J. Blundell, Phys. Rev. B **84**, 144416 (2011).
[17] K.-W. Lee and W. E. Pickett, Europhys. Lett. **80**, 37008 (2007).
[18] S. Gangopadhyay and W. E. Pickett, Phys. Rev. B **91**, 045133 (2015).
[19] S. Gangopadhyay and W. E. Pickett, Phys. Rev. B **93**, 155126 (2016).
[20] L. Lu, M. Song, W. Liu, A. P. Reyes, P. Kuhns, H. O. Lee, I. R. Fisher, and V. F. Mitrović, Nat. Commun. **8**, 14407 (2017).
[21] T. Aharen, J. E. Greedan, C. A. Bridges, A. A. Aczel, J. Rodriguez, G. MacDougall, G. M. Luke, T. Imai, V. K. Michaelis, S. Kroeker, H. Zhou, C. R. Wiebe, and L. M. D. Cranswick, Phys. Rev. B **81**, 224409 (2010).
[22] M. A. de Vries, A. C. Mclaughlin, and J.-W. G. Bos, Phys. Rev. Lett. **104**, 177202 (2010).
[23] M. de Vries, J. Piatek, M. Misek, J. Lord, H. Rnnow, and J.-W. G. Bos, New J. Phys. **15**, 043024 (2013).
[24] A. C. Mclaughlin, M. A. de Vries, and J.-W. G. Bos, Phys. Rev. B **82**, 094424 (2010).
[25] F. Coomer and E. Cussen, J. Phys. Condens. Matter **25**, 082202 (2013).
[26] W. M. H. Natori, E. C. Andrade, E. Miranda, and R. G. Pereira, Phys. Rev. Lett. **117**, 017204 (2016).
[27] A. Abragam and B. Bleaney, *Electron Paramagnetic Resonance of Transition Ions* (Clarendon Press, Oxford, 1970).
[28] Recent *ab initio* study of $Ba_2YMoO_6$ suggests $t \simeq 0.15$ eV and order of magnitude smaller NN off diagonal as well as further neighbor hopping amplitudes; S. Streltsov (private communication).
[29] The parameters $t \simeq 0.12$–$0.15$ eV [15,28] and $U \simeq 2$–$3$ eV [15,30] have been suggested for molybdenum and osmium double perovskites. We thus estimate $t/U \sim 0.04$–$0.07$ that is small enough to justify our perturbative $t/U$ expansion up to leading order.
[30] L. Vaugier, H. Jiang, and S. Biermann, Phys. Rev. B **86**, 165105 (2012).
[31] $r_1 = 1/(1-3\eta)$, $r_2 = 1/(1-\eta)$, and $r_3 = 1/(1+2\eta)$.
[32] See Supplemental Material at http://link.aps.org/supplemental/10.1103/PhysRevLett.118.217202 for the details.
[33] G. Jackeli and D. A. Ivanov, Phys. Rev. B **76**, 132407 (2007).
[34] A similar representation has been used in Ref. [26].
[35] T. Senthil, A. Vishwanath, L. Balents, S. Sachdev, and M. P. A. Fisher, Science **303**, 1490 (2004).
[36] J. P. Carlo, J. P. Clancy, T. Aharen, Z. Yamani, J. P. C. Ruff, J. J. Wagman, G. J. Van Gastel, H. M. L. Noad, G. E. Granroth, J. E. Greedan, H. A. Dabkowska, and B. D. Gaulin, Phys. Rev. B **84**, 100404 (2011).
[37] Z. Qu, Y. Zou, S. Zhang, L. Ling, L. Zhang, and Y. Zhang, J. Appl. Phys. **113**, 17E137 (2013).
[38] P. M. M. Thygesen, J. A. M. Paddison, R. Zhang, K. A. Beyer, K. W. Chapman, H. Y. Playford, M. G. Tucker, D. A. Keen, M. A. Hayward, and A. L. Goodwin, Phys. Rev. Lett. **118**, 067201 (2017).